Proceedings of the ASME 2018 International Design Engineering Technical Conferences and Computers and Information in Engineering Conference
IDETC2018
August 26-29, 2018, Quebec City, Quebec, Canada

DETC2018-85616

NUMERICAL COMPUTATION OF THE DISCRETE 2D FOURIER TRANSFORM IN POLAR COORDINATES

Xueyang Yao
Department of Mechanical Engineering
University of Ottawa
Ottawa, Ontario, Canada

Natalie Baddour
Department of Mechanical Engineering
University of Ottawa
Ottawa, Ontario, Canada

ABSTRACT

The discrete Fourier transform in Cartesian coordinates has proven to be invaluable in many disciplines. However, in application such as photoacoustics and tomography, a discrete 2D-Fourier transform in polar coordinates is needed. In this paper, a discrete 2D-Fourier transform in polar coordinates is presented. It is shown that numerical implementation is best achieved by interpreting the transform as a 1D-discrete Fourier transform (DFT), a 1D-discrete Hankel transform (DHT) and a 1D-discrete inverse transform (IDFT) in sequence. The transform is tested by numerical simulations with respect to accuracy and precision for computation of the continuous 2D transform at specific discrete points. It was found that both the forward and inverse transform showed good accuracy to approximate the continuous Fourier transform. Moreover, good precision results were obtained, which indicate that the proposed transform itself does not add much error.

NOMENCLATURE

f_{pk}	Sampled original function in polar coordinates
F_{ql}	Discrete 2D Fourier transform in polar coordinates
N_1	Sample size in radial direction
N_2	Sample size in angular direction
r_{pk}	Sample point in radial direction in space domain
θ_p	Sample point in angular direction in space domain
ρ_{ql}	Sample point in radial direction in frequency domain
ψ_q	Sample point in angular direction in frequency domain
R	Effective space limit
W_p	Effective band limit
$E(v)$	Dynamic error to test the accuracy
ε	Average of absolute error to test precision

INTRODUCTION

The Fourier transform is a powerful analytical tool and has proven to be invaluable in many disciplines such as physics, mathematics and engineering. The development of the Fast Fourier Transform (FFT) algorithm [1], which computes the discrete Fourier transform with a fast algorithm, established the Fourier transform as a practical tool in diverse application areas, most notably signal and image processing.

In 2D, the FFT algorithm can still be used in Cartesian coordinates, by implementing two discrete 1D transforms. However, in many applications, functions are best described in polar coordinates instead of using Cartesian coordinates. For example, there have been applications to photoacoustics [2], tomography ([3], [4], [5]) and scattering problem([6], [7], [8]) where a discrete 2D-Fourier transform in polar coordinates is needed. Moreover, for functions that are naturally described in polar coordinates, a discrete version of the 2D Fourier transform in polar coordinates is needed.

There have been other attempts to calculate a discrete 2D-Fourier transform in polar coordinates, such as Nonequally spaced FFTs (NUFFT, see [9], [10], [11], [12]) and Pseudo-Polar Fourier transform ([13], [14], [15]). However, these prior works focused on numerical approximation of the continuous transform, rather than the development and evaluation of a discrete transform that possesses its own set of operational rules and can exist as a discrete transform in its own right. This stands in contrast to approaches that have been taken

with the continuous/discrete Fourier transform where the Discrete Fourier Transform (DFT) exists as its own transform with its own set of operational rules, in addition to its utility at approximating the continuous version of the Fourier transform.

In [16] and [17], Baddour demonstrated that the continuous 2D-Fourier transform in polar coordinates can be interpreted as a continuous 1D-Fourier transform, a continuous 1D-Hankel transform and a continuous inverse 1D-Fourier transform in sequence. In this paper, a discrete 2D Fourier transform in polar coordinates is proposed and implemented as a sequence of 1D discrete Fourier, Hankel and Inverse Fourier transforms, similar to the sequence of transform that make up the continuous 2D Fourier transform in polar coordinates. The ability of the proposed transform to be used to numerically evaluate the continuous transform at specific points is subsequently evaluated.

INTERPRETATION OF THE 2D FORWARD DFT IN POLAR COORDINATES

In this paper, we propose a definition of the 2D-Discrete Fourier Transform in polar coordinates as the discrete transform that transforms the matrix (or double-subscripted series f_{pk} to the matrix (double-subscripted series) to the matrix F_{ql} according to

$$F_{ql} = \mathbb{F}\left(f_{pk}\right) \tag{1}$$

where

$$F_{ql} = \frac{1}{N_2}\sum_{n=-M}^{M} e^{+in\frac{2\pi q}{N_2}} i^{-n} \sum_{k=1}^{N_1-1} \frac{2J_n\left(\frac{j_{nk}\,j_{nl}}{j_{nN_1}}\right)}{j_{nN_1}J_{n+1}^2\left(j_{nk}\right)} \left\{\sum_{p=-M}^{M} f_{pk} e^{-in\frac{2\pi p}{N_2}}\right\} \tag{2}$$

where p, k, q, l, n, N_1 and N_2 are integers such that $2M+1=N_2$, $1\le l,k,\le N_1-1$ and $-M\le p,q,n\le M$. The integers N_1 and N_2 represent the size of the spaces in which we work, with N_2 representing the dimension in the angular direction and N_1 represents the dimension in the radial direction.

We can think of these as a series of 1D discrete Fourier transforms along with a discrete Hankel transform in the following way. The first step is a forward 1D DFT transforming $f_{pk}\to\overline{f}_{nk}$ where the p subscript is transformed to the n subscript:

$$\overline{f}_{nk} = \sum_{p=-M}^{M} f_{pk} e^{-in\frac{2\pi p}{N_2}} \qquad \text{for } n=-M..M,\ k=1..N_1-1 \tag{3}$$

The overbar is used to indicate a standard 1D DFT. In matrix operations, this is equivalent to stating that each *column* of f_{pk} is DFT'ed to yield $\overline{f}_{nk}$. The second step of equation (2) is a discrete Hankel transform of order n, transforming $\overline{f}_{nk}\to\hat{\overline{f}}_{nl}$ so that the k subscript is Hankel transformed to the l subscript via

$$\hat{\overline{f}}_{nl} = \sum_{k=1}^{N_1-1} \frac{2J_n\left(\frac{j_{nk}\,j_{nl}}{j_{nN_1}}\right)}{j_{nN_1}J_{n+1}^2\left(j_{nk}\right)} \overline{f}_{nk} \qquad \text{for } n=-M..M,\ l=1..N_1-1 \tag{4}$$

The overhat is used to indicate a Discrete Hankel Transform (DHT), with the DHT as defined in [18]. Using the same transformation matrix notation defined in [18], we define the transformation matrix

$$Y_{l,k}^{nN_1} = \frac{2}{j_{nN_1}J_{n+1}^2\left(j_{nk}\right)} J_n\left(\frac{j_{nl}\,j_{nk}}{j_{nN_1}}\right) \qquad 1\le l,k\le N_1-1 \tag{5}$$

Hence equation (4) can be written as

$$\hat{\overline{f}}_{nl} = \sum_{k=1}^{N_1-1} Y_{l,k}^{nN_1}\,\overline{f}_{nk} \qquad \text{for } n=-M..M,\ l=1..N_1-1 \tag{6}$$

In matrix operations, this states that each *row* of $\overline{f}_{nk}$ is DHT'ed to yield $\hat{\overline{f}}_{nl}$. These are now scaled to give the Fourier coefficients of the 2D DFT $\hat{\overline{f}}_{nl}\to\overline{F}_{nl}$ such that

$$\overline{F}_{nl} = i^{-n}\hat{\overline{f}}_{nl} = i^{-n}\sum_{k=1}^{N_1-1} Y_{l,k}^{nN_1}\,\overline{f}_{nk} \qquad \text{for } n=-M..M,\ l=1..N_1-1 \tag{7}$$

It is noted that the step in equation (7) exactly parallels the continuous form equivalent step where $F_n(\rho)=2\pi\, i^{-n}\mathbb{H}_n\left\{f_n(r)\right\}$, see [16].

The final step of the forward 2D DFT in polar coordinates is then a standard *inverse* 1D DFT, which transforms each *column* of $\overline{F}_{nl}\to F_{ql}$ so that the n subscript is (inverse) transformed to the q subscript via

$$F_{ql} = \frac{1}{N_2}\sum_{n=-M}^{M} \overline{F}_{nl} e^{+in\frac{2\pi q}{N_2}} \qquad \text{for } q=0..N_2-1,\ l=1..N_1-1 \tag{8}$$

This is pointed out since it was shown in [16], [17] that a continuous 2D Fourier transform in polar coordinates is precisely a combination of a Fourier series transform (seen as a transform, transforming the continuous function to its discrete set of Fourier coefficients), a Hankel transform for each Fourier coefficient and then an inverse Fourier series transform (transforming a set of Fourier coefficients back to a continuous function by via the infinite Fourier series summation). Hence, it has been shown here that the proposed 2D-DFT in polar coordinates is also composed of the same group of transformations: a forward DFT, a forward DHT and then an inverse DFT.

INTERPRETATION OF THE 2D INVERSE DFT IN POLAR COORDINATES

Similarly, the inverse 2D-DFT in polar coordinates is define as the transformation from F_{ql} back to f_{pk} as

$$f_{pk} = \mathbb{F}^{-1}\left(F_{ql}\right) \tag{9}$$

where

$$f_{pk} = \frac{1}{N_2}\sum_{n=-M}^{M} i^n e^{+i\frac{2\pi np}{N_2}} \sum_{l=1}^{N_1-1} \frac{2J_n\left(\frac{j_{nl}\, j_{nk}}{j_{nN_1}}\right)}{j_{nN_1} J_{n+1}^2\left(j_{nl}\right)} \left\{ \sum_{q=-M}^{M} F_{ql} e^{-i\frac{2\pi nq}{N_2}} \right\} \tag{10}$$

The steps of the inverse 2D DFT are the reverse steps outlined above for the forward 2D DFT. First $F_{ql} \to \bar{F}_{nl}$ via a forward 1D DFT

$$\bar{F}_{nl} = \sum_{q=M}^{M} F_{ql} e^{-i\frac{2\pi nq}{N_2}} \qquad n = -M..M,\ \ l = 1..N_1 - 1 \tag{11}$$

Then a discrete Hankel transform to obtain $\bar{F}_{nl} \to \hat{\bar{F}}_{nk}$

$$\hat{\bar{F}}_{nk} = \sum_{l=1}^{N_1-1} \frac{2J_n\left(\frac{j_{nl}\, j_{nk}}{j_{nN_1}}\right)}{j_{nN_1} J_{n+1}^2\left(j_{nl}\right)} \bar{F}_{nl} \qquad \text{for } n = -M..M,\ \ k = 1..N_1 - 1 \tag{12}$$

Equation (12) can be written as

$$\hat{\bar{F}}_{nk} = \sum_{l=1}^{N_1-1} Y_{k,l}^{nN_1} \bar{F}_{nl} \qquad \text{for } n = -M..M,\ \ k = 1..N_1 - 1 \tag{13}$$

Followed by a scaling operation to obtain $\hat{\bar{F}}_{nk} \to \bar{f}_{nk}$

$$\bar{f}_{nk} = i^{+n} \hat{\bar{F}}_{nk} \qquad \text{for } n = -M..M,\ \ k = 1..N_1 - 1 \tag{14}$$

Again, the step in equation (14) parallels the continuous form equivalent which is given by $f_n(r) = \frac{i^n}{2\pi}\,\mathbb{H}_n\left\{F_n(\rho)\right\}$, see[16].

Then, finally an inverse 1D IDFT is used to obtain $\bar{f}_{nk} \to f_{pk}$

$$f_{pk} = \frac{1}{N_2}\sum_{n=-M}^{M} \bar{f}_{nk} e^{+i\frac{2\pi np}{N_2}} \qquad \text{for } p = -M..M,\ \ k = 1..N_1 - 1 \tag{15}$$

For both forward and inverse 2D-DFT, the sequence of operations is a DFT of each column of the starting matrix, followed by a DHT of each row, a term-by-term scaling, followed by an IDFT of each column.

DISCRETIZATION POINTS

Function limits

Let us consider any function in continuous 2D space. A function cannot be limited in both space and spatial frequency (spatial frequency is the frequency domain when the pre-transform variables are considered as space variables rather than the usual temporal variables). When implementing a discrete transform for application to a function in continuous 2D space, it is necessary to truncate the function somewhere in both domains so that after the truncation points, the amplitude of the function could be seen as zero or effectively zero. Therefore the concept of effective limit is used here. A function is defined as being 'effectively limited in space by R' means that if $r > R$, then as $r \to \infty$, $f(r) \to 0$ or in other words, the function can be made arbitrarily small or as close to zero as necessary for all $r > R$. The same idea can be applied to the frequency domain.

Space limited function

We assume that the original function that we are interested in is defined over continuous (r,θ) space where $0 \le r \le R$ and $0 \le \theta \le 2\pi$. Because of periodicity of the functions in the angular direction, the sample points in both space and frequency domains are chosen as equally spaced in the angular direction, as is always the case for a discrete 1D Fourier transform. In the radial direction, since a discrete Hankel transform is being implemented, the sample points as defined in [18] are used. Therefore, the sampling spaces used for radial and angular sampling points in regular $\vec{r}$ space (r,θ) and $\vec{\omega}$ frequency (ρ,ψ) space are defined as

$$r_{pk} = \frac{j_{pk} R}{j_{pN_1}} \qquad \theta_p = \frac{p2\pi}{N_2} \tag{16}$$

and

$$\rho_{ql} = \frac{j_{ql}}{R} \qquad \psi_q = \frac{q2\pi}{N_2} \tag{17}$$

Equations (16) and (17) give the sampling grid in regular (r,θ) and frequency (ρ,ψ) space. Clearly, the density of the sampling points depends on the numbers of points chosen, that is on N_1 and N_2. Also clear is the fact that the grid is not equi-spaced in the radial variable. The sampling grids are plotted below to enable visualization. In the first instance, the polar grids are plotted for the case $R = 1$, $N_1 = 16$ and $N_2 = 15$. These are shown in space (***r*** space) and frequency (***ρ*** space) in Figure 1and Figure 2 respectively.

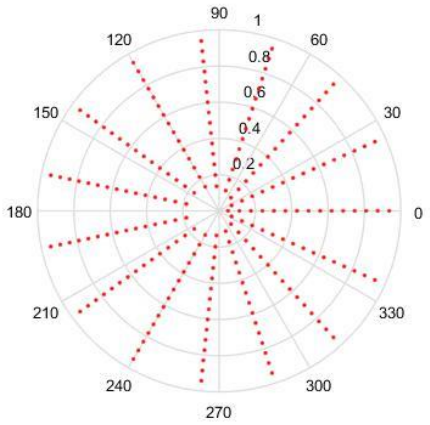

Figure 1 Sampling grid in space domain of a space limited function for R=1, N_1=16 and N_2 = 15

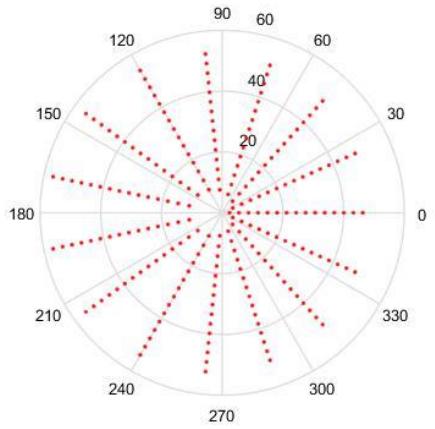

Figure 2 Sampling grid in frequency domain of a space limited function for R=1, N_1=16 and N_2 = 15

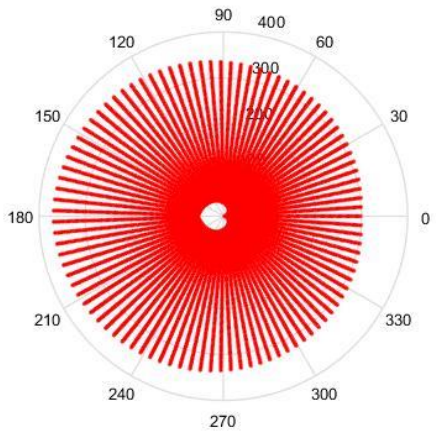

Figure 3 Sampling grid in space domain of a band limited function for W_p=1, N_1=96 and N_2 = 95

Band limited function

Consider the case of a bandlimited functions, such that the function is defined over continuous (ρ,ψ) space where $0 \le \rho \le W_p$ and $0 \le \psi \le 2\pi$ and is effective zero elsewhere (that is, the function can be made as close to zero as necessary, elsewhere in the plane). Similar to the space limited function, the sample points in angular direction are chosen as equispaced and the sample points in radial direction are as defined in [18]. The sampling space used for radial and angular sampling points in regular $\vec{\omega}$ frequency space (ρ,ψ) and $\vec{r}$ space (r,θ) for a bandlimited function are defined as

$$r_{pk} = \frac{j_{pk}}{W_p} \qquad \theta_p = \frac{p2\pi}{N_2} \tag{18}$$

and

$$\rho_{ql} = \frac{j_{ql} W_p}{j_{qN_1}} \qquad \psi_q = \frac{q2\pi}{N_2} \tag{19}$$

It can be observed that the sampling points of a frequency limited function are similarly structured to the ones for a space limited function. Hence, the sampling grid should have same shape as before but with the domains reversed (that is, the shape of the spatial grid for the bandlimited function resembles the frequency grid of the space-limited function and vice versa). The sampling grids are shown in Figure 3 and Figure 4. In the case, the polar grids are plotted for the case $W_p = 1, N_1 = 96$ and $N_2 = 95$.

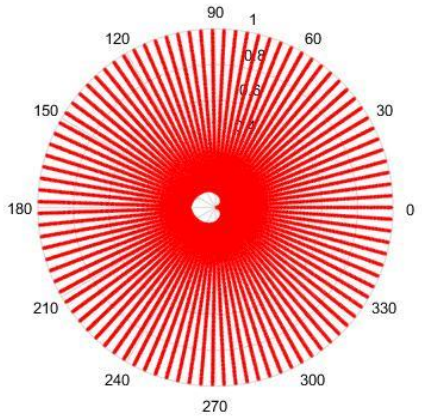

Figure 4 Sampling grid in frequency domain of a band limited function for W_p=1, N_1=96 and N_2 = 95

It can be observed that the sample grid for a band limited function has the same shape as with space limited function but the domains are switched. Moreover, the sample grid for a band /space limited function suffers from the problem that there is a heart-shaped area in the centre that is not be covered by the sample grid.

DISCRETE 2D FOURIER TRANSFORM TEST AND RESULTS

Method for testing the Algorithm

In this section, the ability of the 2D discrete Fourier transform is evaluated for its ability to estimate the continuous Fourier transform at the selected special sampling points in the spatial and frequency domains.

1) ***Accuracy***

In order to test the accuracy of the 2D-DFT and 2D-IDFT to calculate the continuous counterpart, the dynamic error has been used. It is defined as [19]

$$E(\mathrm{v}) = 20\log_{10}\left[\frac{|C(\mathrm{v}) - D(\mathrm{v})|}{\max|D(\mathrm{v})|}\right] \tag{20}$$

where $C(\mathrm{v})$ is the continuous forward or inverse 2D-Fourier transform and $D(\mathrm{v})$ is the values obtained from the discrete counterpart. The dynamic error is defined as the ratio of the absolute error to the maximum amplitude of the function, which is calculated on a log scale. Therefore, a large negative value represents an accurate discrete transform. The dynamic error is used instead of the percentage error in order to avoid division by zero.

2) ***Precision***

The precision of the algorithm is another important evaluation criterion, which is tested by sequentially performing a pair of forward and inverse transforms and comparing the result to the original function. High precision indicates that the transform does not add much error by the calculations. An average of absolute error of each sample points between the original function and the calculated counterpart was used to measure the precision. It is given by

$$\varepsilon = \frac{1}{(N_1 - 1)\cdot N_2}\sum_{n=1}^{(N_1-1)\cdot N_2}\left|f - f^*\right| \tag{21}$$

where f is the original function and f^* is the calculated counterpart. An ideal precision would result in the absolute error being zero.

Test Functions

1) Four-term sinusoid and modified exponential

The first test function is given by

$$f(r,\theta) = \frac{\mathrm{e}^{-ar}}{r}[3\sin(\theta) + \sin(3\theta) + 4\cos(10\theta) + 12\sin(15\theta)] \tag{22}$$

Its continuous 2D-FT can be calculated as

$$F(\rho,\psi) = -6\pi i\sin(\psi)\frac{\sqrt{\rho^2+a^2}-a}{\rho\sqrt{\rho^2+a^2}} + 2\pi i\sin(3\psi)\frac{(\sqrt{\rho^2+a^2}-a)^3}{\rho^3\sqrt{\rho^2+a^2}}$$
$$-8\pi\cos(10\psi)\frac{(\sqrt{\rho^2+a^2}-a)^{10}}{\rho^{10}\sqrt{\rho^2+a^2}} + 24\pi i\sin(15\psi)\frac{(\sqrt{\rho^2+a^2}-a)^{15}}{\rho^{15}\sqrt{\rho^2+a^2}} \tag{23}$$

The graphs for the original function and its continuous 2D-DFT with $a = 1$ and shown in Figure 5.

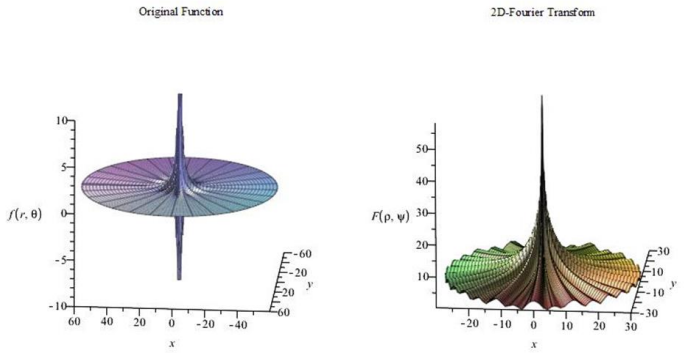

Figure 5 Original function and its 2D-Fourier transform of 'Four-term Sinusoid & Modified Exponential' function

From Figure 5, it can be assumed that $f(r,\theta)$ is effectively space-limited from $R = 40$ and $F(\rho,\psi)$ is effectively band-limited with $W_p = 30$,which gives $j_{0N_1} \approx 1200$ [18]. This results in $N_1 = 383$.

In the angular direction, the highest frequency term is $12\sin(15\theta)$. From the sampling theorem [20], the sampling frequency should be at least twice of the highest frequency of signal. Thus $N_2 = 41$ is chosen.

*a) **Forward Transform***

Test results for the forward transform are shown in Figure 6 and Figure 7. The error gets bigger at the center as expected. However, the maximum value of the error is $Error_{\max} = -10.1535dB$ and this occurs at the center. The average value of the error is $Error_{average} = -32.7619dB$.

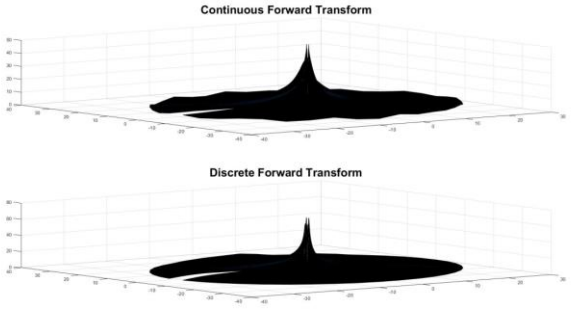

Figure 6 Continuous forward transform and discrete forward transform of 'Four-term Sinusoid & Modified Exponential' function with R=40, W_p=30, N_1=383, N_2=41

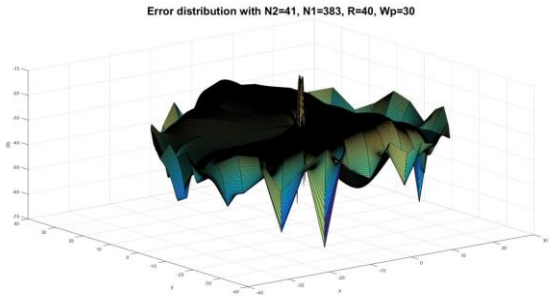

Figure 7 Error distribution of the forward transform of 'Four-term Sinusoid & Modified Exponential' function with R=40, W_p=30, N_1=383, N_2=41

*b) **Inverse Transform***

Figure 8 and Figure 9 show the test results for the inverse transform. The maximum value of the error is $Error_{\max} = 0.5579dB$ and this occurs at the center. The average of the error is $Error_{average} = -68.7317dB$.

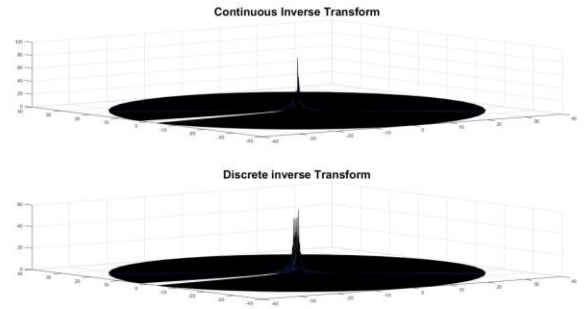

Figure 8 Continuous inverse transform and discrete forward transform of 'Four-term Sinusoid & Modified Exponential' function with R=40, W_p=30, N_1=383, N_2=41

.

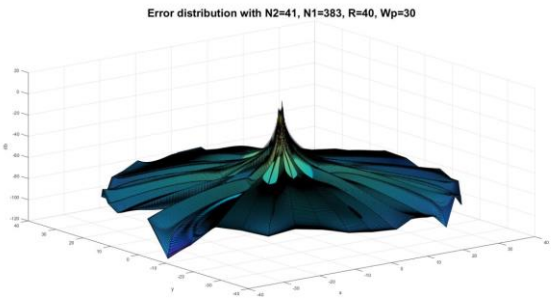

Figure 9 Error distribution of the inverse transform of 'Four-term Sinusoid & Modified Exponential' function with R=40, W_p=30, N_1=383, N_2=41

Performing sequential 2D-DFT and 2D-IDFT results in $\varepsilon = 1.421 \times e^{-12}$ where ε is calculated with (21). Therefore, sequentially performing the forward and inverse transforms does not add much error to the computation

2) Four-term sinusoid & Sinc Function

The second chosen function is given as

$$f(r,\theta) = \frac{\sin(ar)}{ar}[3\sin(\theta) + \sin(3\theta) + 4\cos(10\theta) + 12\sin(15\theta)] \quad (24)$$

which is a sinc function in the radial direction and a four-term sinusoid in angular direction. The continuous 2D-FT can be calculated as

$$F(\rho,\psi) = \begin{cases} \dfrac{8\pi\cos(10\psi)\rho^{10}}{a\sqrt{a^2-\rho^2}\,(a+\sqrt{a^2-\rho^2})^{10}}, & \rho < a \\ -\dfrac{6\pi I\sin(\psi)}{a\rho\sqrt{\rho^2+a^2}} + \dfrac{2\pi I\sin\left(3\arcsin\left(\dfrac{a}{\rho}\right)\right)\sin(3\psi)}{\sqrt{\rho^2+a^2}} \\ -\dfrac{8\pi\sin\left(10\arcsin\left(\dfrac{a}{\rho}\right)\right)\cos(10\psi)}{\sqrt{\rho^2+a^2}} \\ +\dfrac{24\pi I\sin\left(15\arcsin\left(\dfrac{a}{\rho}\right)\right)\sin(15\psi)}{\sqrt{\rho^2+a^2}}, & \rho > a \end{cases} \quad (25)$$

The graphs for the original function and its continuous 2D-FT with $a = 5$ are shown in Figure 10.

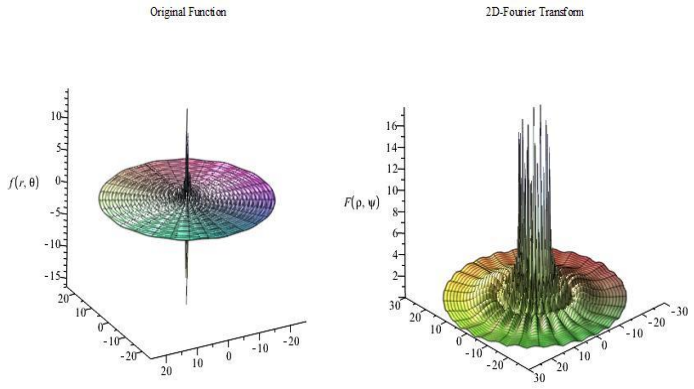

Figure 10 Original Function and its 2D-Fourier transform for the 'Four-term Sinusoid & Sinc' function

In the radial direction, from the graphs of the original function and its 2D-FT, it can be assumed that $f(r,\theta)$ is space-limited at $R = 15$ and band-limited at $W_p = 90$, which gives $j_{0N_1} \approx 1350$ [18]. This results in $N_1 = 430$.

In the angular direction, the highest frequency term is $12\sin(15\theta)$. From the sampling theorem, the sampling

frequency should be at least twice that of the highest frequency present in the signal. Thus, $N_2 = 41$ is chosen. The function will be tested as a band-limited function.

a) Forward Transform

Test results for the forward transform are shown in Figure 11 and Figure 12 The maximum value of the error is $Error_{\max} = 10.6535dB$ and this occurs where the discontinuities are located. The average of the error is $Error_{average} = -38.7831dB$.

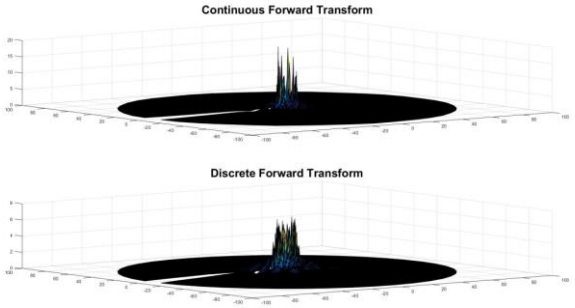

Figure 11 Sampled continuous forward transform and discrete forward transform of 'Four-term sinusoid & Sinc' Function with R=15,W_p=90,N_1=430, N_2=41

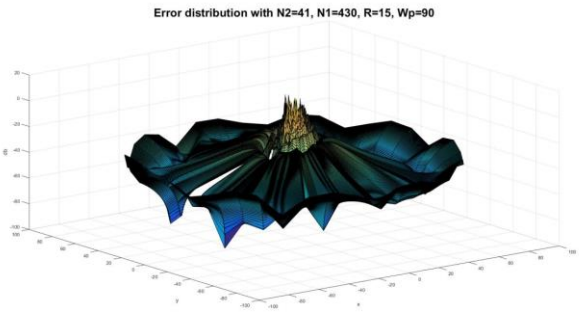

Figure 12 Error distribution of the forward transform of 'Four-term sinusoid & Sinc' Function with R=15,W_p=90,N_1=430, N_2=41

b) Inverse Transform

Figure 13 and Figure 14 show the test result for the inverse transform. The maximum value of the error is $Error_{\max} = -8.6734dB$ .The average of the error is $Error_{average} = -37.8119dB$.

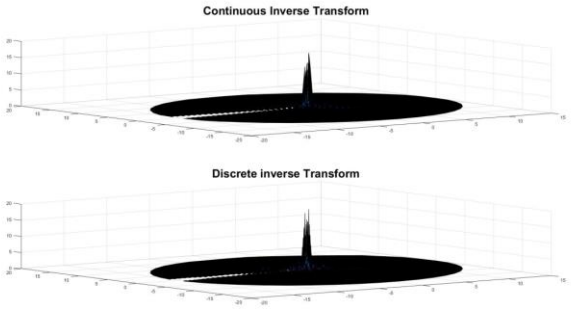

Figure 13 Sampled continuous inverse transform and discrete inverse transform of 'Four-term sinusoid & Sinc' Function with R=15,W_p=90,N_1=430, N_2=41

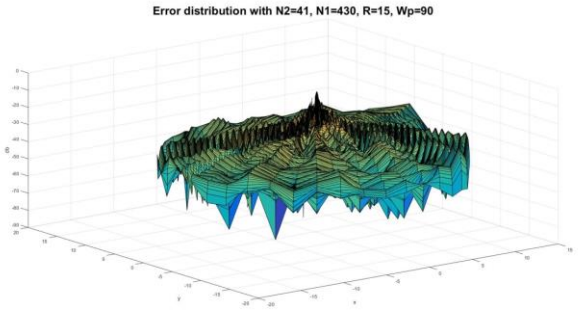

Figure 14 Error distribution of the inverse transform of 'Four-term sinusoid & Sinc' Function with R=15,W_p=90,N_1=430, N_2=41

Performing sequential 2D-DFT and 2D-IDFT results in $\varepsilon = 1.3117 \times e^{-12}$ where ε is calculated with (21). Therefore, performing forward and inverse transform does not add much error.

Discussion of the Tests Results

From the first test case, the forward transform gives an average of error $Error_{average} = -32.7619dB$ which is acceptable. The inverse transform shows a better result which gives an average of error $Error_{average} = -68.7317dB$. For the second test case, the forward transform gives an average of the error $Error_{average} = -38.7831dB$. The result of inverse transform is not as good as the first test case as expected because of the discontinuity. However, $Error_{average} = -37.8119dB$ is still an acceptable approximation. Moreover, for both cases, the value of ε is very close to zero, which verifies that the transform does not add too much error by itself.

SUMMARY AND CONCLUSION

In this paper, a discrete 2D Fourier transform in polar coordinates was presented and subsequently evaluated for accuracy to compute the continuous 2D transform at specific

discretization points. Two test functions were used to evaluate both accuracy and precision of the proposed discrete transform. From the two test cases, both the forward and inverse transform showed good accuracy to approximate the continuous Fourier transform. Moreover, the good precision results indicated that the transform itself does not add much error.

REFERENCES

[1] J. W. Cooley and J. W. Tukey, "An Algorithm for the Machine Calculation of Complex Fourier Series," *Math. Comput.*, vol. 19, no. 90, pp. 297–301, 1965.

[2] Y. Xu, D. Feng, and L. V. Wang, "Exact frequency-domain reconstruction for thermoacoustic tomography. I. Planar geometry," *Med. Imaging IEEE Trans. On*, vol. 21, no. 7, pp. 823–828, 2002.

[3] M. C. Scott *et al.*, "Electron tomography at 2.4-ångström resolution," *Nature*, vol. 483, no. 7390, p. 444, Mar. 2012.

[4] B. P. Fahimian *et al.*, "Radiation dose reduction in medical x-ray CT via Fourier-based iterative reconstruction," *Med. Phys.*, vol. 40, no. 3, p. n/a-n/a, Mar. 2013.

[5] E. Lee *et al.*, "Radiation dose reduction and image enhancement in biological imaging through equally-sloped tomography," *J. Struct. Biol.*, vol. 164, no. 2, pp. 221–227, 2008.

[6] A. Liemert and A. Kienle, "Light transport in three-dimensional semi-infinite scattering media," *JOSA A*, vol. 29, no. 7, pp. 1475–1481, Jul. 2012.

[7] A. Liemert and A. Kienle, "Radiative transfer in two-dimensional infinitely extended scattering media," *J. Phys. Math. Theor.*, vol. 44, no. 50, p. 505206, 2011.

[8] "Sensitivity kernels for coda-wave interferometry and scattering tomography: theory and numerical evaluation in two-dimensional anisotropically scattering media | Geophysical Journal International | Oxford Academic." [Online]. Available: https://academic.oup.com/gji/article-abstract/204/1/650/636209. [Accessed: 04-May-2018].

[9] E. Suli and A. Ware, "A Spectral Method of Characteristics for Hyperbolic Problems," *SIAM J. Numer. Anal.*, vol. 28, no. 2, pp. 423–445, 1991.

[10] A. Dutt and V. Rokhlin, "Fast Fourier Transforms for Nonequispaced Data," *SIAM J. Sci. Comput.*, vol. 14, no. 6, pp. 1368–1393, Nov. 1993.

[11] C. Anderson and M. Dahleh, "Rapid Computation of the Discrete Fourier Transform," *SIAM J. Sci. Comput.*, vol. 17, no. 4, pp. 913–919, Jul. 1996.

[12] A. F. Ware, "Fast Approximate Fourier Transforms for Irregularly Spaced Data," *SIAM Rev.*, vol. 40, no. 4, p. 838, Dec. 1998.

[13] A. Averbuch, R. R. Coifman, D. L. Donoho, M. Elad, and M. Israeli, "Fast and accurate Polar Fourier transform," *Appl. Comput. Harmon. Anal.*, vol. 21, no. 2, pp. 145–167, 2006.

[14] A. Averbuch, G. Shabat, and Y. Shkolnisky, "Direct Inversion of the Three-Dimensional Pseudo-polar Fourier Transform," *SIAM J. Sci. Comput.*, vol. 38, no. 2, pp. A1100–A1120, Jan. 2016.

[15] A. Averbuch, R. R. Coifman, D. L. Donoho, M. Israeli, and Y. Shkolnisky, "A Framework for Discrete Integral Transformations I-the Pseudopolar Fourier Transform," *SIAM J. Sci. Comput.*, vol. 30, no. 2, pp. 764–784, Feb. 2008.

[16] N. Baddour, "Two-Dimensional Fourier Transforms in Polar Coordinates," *Adv. Imaging Electron Phys.*, vol. 165, pp. 1–45, Jan. 2011.

[17] N. Baddour, "Operational and convolution properties of two-dimensional Fourier transforms in polar coordinates," *JOSA A*, vol. 26, no. 8, pp. 1767–1777, Aug. 2009.

[18] N. Baddour and U. Chouinard, "Theory and operational rules for the discrete Hankel transform," *JOSA A*, vol. 32, no. 4, pp. 611–622, Apr. 2015.

[19] A. Agnesi, G. C. Reali, G. Patrini, and A. Tomaselli, "Numerical evaluation of the Hankel transform: remarks," *JOSA A*, vol. 10, no. 9, pp. 1872–1874, Sep. 1993.

[20] C. E. Shannon, "Communication in the presence of noise," *Proc. IEEE*, vol. 72, no. 9, pp. 1192–1201, 1984.